The Journal of Chemical Physics

Kinetic phase diagram for CO oxidation on Pt(210): Pattern formation in the hysteresis and oscillation regions

Cite as: J. Chem. Phys. **106**, 4291 (1997); https://doi.org/10.1063/1.473131
Submitted: 15 May 1995 . Accepted: 14 October 1996 . Published Online: 04 June 1998

Martin Berdau, Andrzej Karpowicz, Georgii G. Yelenin, Klaus Christmann, and Jochen H. Block

View Online Export Citation

ARTICLES YOU MAY BE INTERESTED IN

Oscillatory CO oxidation on Pt(110): Modeling of temporal self-organization
The Journal of Chemical Physics **96**, 9161 (1992); https://doi.org/10.1063/1.462226

Reaction diffusion patterns in the catalytic CO-oxidation on Pt(110): Front propagation and spiral waves
The Journal of Chemical Physics **98**, 9977 (1993); https://doi.org/10.1063/1.464323

Mechanisms of spatial self-organization in isothermal kinetic oscillations during the catalytic CO oxidation on Pt single crystal surfaces
The Journal of Chemical Physics **90**, 510 (1989); https://doi.org/10.1063/1.456501

Challenge us.
What are your needs for periodic signal detection?
Watch

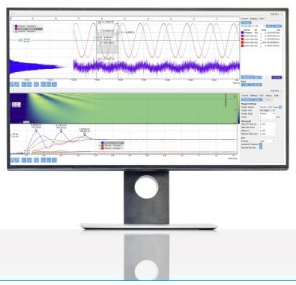

Zurich Instruments

AIP Publishing

© 1997 American Institute of Physics.

Kinetic phase diagram for CO oxidation on Pt(210): Pattern formation in the hysteresis and oscillation regions

Martin Berdau, Andrzej Karpowicz,[a] Georgii G. Yelenin,[b] Klaus Christmann,[c] and Jochen H. Block[d]
Fritz-Haber-Institut der Max-Planck-Gesellschaft, Faradayweg 4-6, D-14195 Berlin, Germany

(Received 15 May 1995; accepted 14 October 1996)

The reactive behavior of catalytic CO oxidation on Pt(210) is studied by means of combined reaction rate measurements and photoelectron emission microscopy (PEEM). These methods allow an investigation of the phenomena at macroscopic and mesoscopic level, respectively. The external control parameters (flow rate, CO and oxygen partial pressures, surface temperature and scanning rates of pressure and temperature) are systematically varied to reveal various reactive regions in parameter space. The *macroscopic* measurements for a given temperature and flow rate (under isothermal conditions) show that *lower pressures* lead to a pronounced *clockwise hysteresis* in the production rate of CO_2, while *increasing* pressures cause a systematic narrowing leading to a crossing of the two hysteresis branches into a region of *counterclockwise hysteresis*. A further pressure increase leads to macroscopic *temporal oscillations*. Mesoscopic *spatiotemporal oscillations* appear at the same conditions. The resulting macroscopic isothermal kinetic phase diagram exhibits a cross-shaped characteristic similar to that previously obtained for the Pd(110) surface. The mesoscopic lateral distribution of CO and oxygen adsorbed on the surface is monitored with the photoelectron emission microscope during the reaction at isothermal conditions and different constant oxygen pressures. The observed mesoscopic spatiotemporal patterns, such as islands, waves, target patterns and spirals, are correlated via the external control parameters with different regions in the macroscopic isothermal phase diagram. The results are compared with previous data of CO oxidation on other surfaces, like Pd(110) and Pt(110). © *1997 American Institute of Physics.* [S0021-9606(97)00104-9]

I. INTRODUCTION

The catalytic CO oxidation by oxygen on Pt metal surfaces (in particular Pt and Pd) can, for a given set of external control parameters, exhibit nonlinear behavior like bistability, self-sustained kinetic oscillations and spatiotemporal patterns, which are indicative of self-organizing processes[1] occurring in the course of the reaction.[2–4] It has turned out, however, from a variety of recent studies which focus either on the observation of temporal oscillations on the macroscopic scale[4,5] or spatiotemporal oscillations on the mesoscopic scale[6–9] that even the supposedly simple heterogeneous CO oxidation holds a complexity that is far from being understood.

In this situation a useful and, in our opinion, necessary aid for any further considerations or suggestions of kinetic models etc. is a reliable chart of the monostable, bistable, and oscillatory regions in parameter space. In other words, any laboratory group that exposes, for instance, a Pd(110) surface to a given mixture of CO and oxygen at a fixed temperature should readily observe the reactive behavior predicted in such a chart for this set of external control parameters.

In a previously published article[5] we reported an experimentally determined macroscopic isothermal kinetic phase diagram for CO oxidation on Pd(110) and could therein clearly separate the regions of monostability, bistability, and temporal oscillations. Since the regions of hysteresis and oscillations reveal a characteristic shape this diagram is referred to as a *cross-shaped phase diagram*.[10] For a detailed description of the term ''phase diagram'' in this context, we refer to the aforementioned previous work on Pd(110) (Ref. 5) and original articles by Schlögl.[11,12]

Recently a variety of experimental systems and theoretical models have been investigated which account for these cross-shaped phase diagrams.[13–16] The present work will restrict its focus to the determination of an isothermal phase diagram based on the macroscopically observable reaction rate averaged over the whole single-crystal plane and its correlation to spatiotemporal patterns on the mesoscopic scale. If the features that make up these structures extend over areas larger than ≈ 10 μm and include areas with different work functions, their spatiotemporal evolution can be effectively observed with the photoelectron emission microscope (PEEM), as shown in previous work.[17,18]

For sake of clarity we divide the experimentally observed oscillations into two classes (without considering Turing structures). *Temporal oscillations* can be observed macroscopically as time-dependent variations in the overall

[a]On leave from Technical University of Wrocław, Wybrzeze Wyspianskiego 27, 50-370 Wrocław, Poland.
[b]Also at: Moscow State University, Department of Computational Mathematics and Cybernetics, Laboratory for Mathematical Modeling in Physics, 119899 Moscow, Russia.
[c]Also at: Freie Universität Berlin, Institut für Physikalische und Theoretische Chemie, Takustr. 3, D-14195 Berlin, Germany.
[d]Deceased.

reaction rate, while during *spatiotemporal* oscillations a temporal change of local concentrations in a given surface element (the coverage of CO and oxygen in this case) occur. Typical examples of spatiotemporal oscillations are trains of traveling waves, target patterns and spirals on a mesoscopic scale. In some cases these spatiotemporal patterns do not produce macroscopically observable oscillations in the product yield due to the lack of large-scale synchronization and the global averaging of different local behavior (reactivities).[6] The macroscopic temporal oscillations would ideally be accompanied by mesoscopic spatially homogeneous behavior (which is never observed in the present system). The experimental criterion for the existence of an oscillatory region in parameter space is the appearance of macroscopic (temporal) oscillation, without considering the spatial behavior.

We regard *every* structure formed in the investigated system as a spatiotemporal pattern. Thus we classify growing islands as spatiotemporal *patterns*, but exactly these structures are excluded from the phenomena termed spatiotemporal *oscillations*. This allows us to distinguish easily between islands as the simplest possible structural pattern, and all other more complex patterns, which result in oscillatory (or cyclical) behavior of local elements (in our case alternating CO and oxygen coverage).

We understand the experimentally obtained macroscopic kinetic phase diagram with a bistable and an oscillatory region in the present context as a cross-shaped phase diagram. Here it should be noted that the behavior of real systems can show spatial differences and can be influenced by inhomogeneities on a mesoscopic and microscopic scale, while the term ''cross-shaped phase diagram'' was introduced with reference to model calculations for ideal systems with spatially homogeneous behavior and without considering the appearance of inhomogeneities.[10] The main characteristic of a cross-shaped phase diagram on the macroscopic scale is the connection between the bistable and oscillatory regions. Since this characteristic is found in our experimentally determined macroscopic kinetic phase diagram, we refer to this diagram as cross-shaped, notwithstanding that the present theory may not be able to describe the observed lateral behavior of the present system on a mesoscopic scale.

To avoid any possible misunderstanding, we also summarize the definitions of terms from nonlinear dynamics as used in this work. To this end we take into consideration the experimental results of the present work, but also findings obtained for the Pt(111) surface which exhibit a surprisingly simple behavior in the catalytic CO oxidation.[19,20] These investigations show that the experimentally observed hysteresis is not well described by simulations used at present.[21–23] A typical approach in model calculations is to use reaction terms to describe *macroscopic* behavior, including bistability, and to simulate *mesoscopic* lateral behavior by adding diffusion terms to the system of equations. Zhdanov and Kasemo[21] considered the CO oxidation on Pt(111) and obtained a *point of equistability*, if they took diffusion terms into account; they conclude that, for a sufficiently slow scan rate of a selected external control parameter, any macroscopic hysteresis must vanish, if the induction time is comparably short and the motion of fronts is fast enough. Contrary to this statement, however, are our own experimental results with Pt(111) (Refs. 19, 20) which clearly reveal a persisting hysteresis even for the slowest attainable scan rates of the external control parameter p_{CO}. Parallel PEEM studies probing the mesoscopic surface structure and composition exhibit a whole region of the selected external control parameter where the velocity of reaction/diffusion fronts reaches zero ($v=0$) leading to absolutely *stationary* fronts. Again, this observation contradicts the results of simulations which yield stationary reaction/diffusion fronts ($v=0$) only at a single point of the selected external control parameter which corresponds to a point of equistability. From this apparent discrepancy we conclude that currently existing models still describe the macroscopic behavior of a reactive system from a too phenomenological point of view, but do not really disclose the physical origin of an experimentally observed hysteresis for sufficiently slow scan rate. As a result, such model simulations may be at variance with the behavior of a real system, in other words, the mesoscopic lateral patterns observed with these systems may significantly deviate from theoretical predictions. It is thereby felt that the influence of mesoscopic and microscopic defects is crucial in that they represent stationary noise which can in turn cause nonpredicted front pinning.[24–26]

Since the experimental definition of the bistable region for Pt(111) (Refs. 19, 20) and Pt(210) seem to be less ambiguous than that derived from previous model calculations [Ref. 27; Pt(111): Ref. 22; Pt(110): Refs. 28, 29; Pt(210): Ref. 30], we distinguish, if it is necessary, between the *computed* and *experimental* bistable region. The computed bistable region (region of assisted nucleation) is defined by saddle-node bifurcations in the so-called S-shaped curve (see, for example, Refs. 21, 22). In contrast to this we define the experimental bistable region in the following way: For all values of the external control parameters located in an *experimental bistable region* of the parameter space the system has two macroscopic stable steady states. The observed macroscopic stable steady state depends on the pretreatment of the system (*how* the bistable region is reached). A transition is observed if a control parameter changes to values at which only the other macroscopic steady state is stable. On a mesoscopic scale islands represent one type of patterns which form during the transition between the stable steady states inside the *computed* bistable region except the *experimental* bistable region. Inside the *experimental* bistable region spatiotemporal patterns are either *not formed experimentally* or have a front velocity of zero. On a macroscopic level the appearance of a clockwise hysteresis with respect to the reaction rate during a sufficiently slow variation of the CO pressure is the experimental indication of the existence of an experimental bistable region. We call that hysteresis *true* which experimentally does remain for sufficiently low scanning rates of pressure or temperature. On the mesoscopic level the experimental bistable region can be delimited by determining the pressure interval in which islands do not appear or change in size.

To describe the experimental bistable region theoretically it is, for example, necessary to consider the influence of mesoscopic and microscopic defects (stationary noise, front pinning).[24–26] Improved mathematical modeling of CO oxidation on Pt(111) and new simulations[31] which have taken into account the nonhomogeneous nucleation show the existence of the experimental bistable region inside the region of assisted nucleation (computed bistability).

The macroscopic temporal oscillations in the CO_2 reaction rate were investigated in detail by Ehsasi *et al.*[32] who determined, among others, the range of external control parameters which lead to oscillations on the Pt(210) surface, namely, $10^{-6} \leqslant p_{CO} \leqslant 10^{-3}$ Torr, $4\times10^{-4} \leqslant p_{O_2} \leqslant 4\times10^{-2}$ Torr, $290 \leqslant T \leqslant 430$ K. In their work Ehsasi *et al.* reported indeed fast macroscopic temporal oscillations with a period of a few seconds, but also slow macroscopic temporal oscillations with a longer period of some hundred seconds. These macroscopic temporal oscillations could also be observed in the present investigations. Since the respective oscillations were characterized in great detail in Ref. 32, we confine ourselves to their mere description here and do not present further experimental information.

During hysteresis measurements for CO oxidation on Pd(110) it was observed, at parameter values for which the hysteresis changes from clockwise to counterclockwise orientation, that an extension of the CO pressure cycling time to much slower scans causes macroscopic temporal oscillations to appear [Fig. 5 in Ref. 5 and unpublished results (Ref. 33)]. A ''crossing'' of the hysteresis from clockwise to counterclockwise orientation is therefore believed to be an indication of the possible existence of macroscopic temporal oscillations. Additionally, at higher pressures, the present system shows a clockwise hysteresis at *fast* scans for external control parameters at which macroscopic temporal oscillations are observed in the reaction rate at *slow* scans.

II. EXPERIMENT

As most of the experimental techniques are described in previous publications, only a brief outline of the setup and the standard methods for monitoring reactive behavior is given in the present work. More detail is provided on the photoelectron emission microscope, which allows surface processes to be directly imaged in real time (video frequency, full frame 40 ms, half frame 20 ms) with lateral resolution in the μm range.

The experiments were performed in a stainless-steel ultrahigh vacuum (UHV) system with an effective volume of approximately 30 ℓ. A sophisticated pressure regulating system described elsewhere[19] allows a precise and reproducible control of the (constant) CO and oxygen partial pressures p_i, while the flow rate F is regulated by means of a gate valve. The sample temperature T could be controlled to within 0.1 K.

The photoelectron emission microscope developed by Engel *et al.*[17] is a useful tool for imaging photoelectron currents for the evaluation of mesoscopic surface defects and adsorbate structures (CO and oxygen islands, waves, target patterns, spirals, etc.). The metal sample is illuminated by $\approx$6.2 eV photons from a 200 W deuterium discharge lamp (Heraeus D 200). The ejected photoelectrons—whose current faithfully follows the work function Φ of the illuminated area—are focused on a channel plate by a three-stage electrostatic lens system and imaged on a phosphorus screen, yielding a maximum spatial resolution of 0.1 μm.[17] Surface regions with a low (high) work function give rise to a large (small) photocurrent and thus bright (dark) image areas. The PEEM images are monitored with a CCD camera and stored on Hi8 videotape (Sony EVO-9500P and EVO-9800P). A frame grabber board and specially developed computer software allow digitization of each video frame and noise reduction in the low intensity portions of single-frame images by averaging over individual frames.

III. RESULTS

The presentation of the results is organized in two main parts. The first part presents the measurements and results which are used to construct the macroscopic isothermal kinetic phase diagram (cross-shaped phase diagram) for CO oxidation on Pt(210). The second part deals with the mesoscopic observations and characterization of the spatiotemporal patterns that appear in certain regions of the macroscopic kinetic phase diagram under well-defined conditions.

A. Macroscopic isothermal phase diagram for CO oxidation on Pt(210)

For the Pd(110) surface a detailed determination has been made in an exemplary way of an experimental kinetic phase diagram over an extended region of the *external control parameters* (flow rate F, CO pressure p_{CO}, oxygen pressure p_{O_2}, and surface temperature T, scanning rate of CO pressure $\beta_{CO}=dp_{CO}/dt$, scanning rate of oxygen pressure β_{O_2}, scanning rate of temperature β_T).[5] For relatively *low pressures* the reactivity of the heterogeneous CO oxidation can exhibit an experimental bistable region for a given set of external control parameters, with pronounced hysteresis phenomena in the CO_2 production rate. During a scan of the CO partial pressure, steep transitions between high and low reactivity occur at different values for increasing ($dp_{CO}/dt>0$) and decreasing CO pressure ($dp_{CO}/dt<0$). At a fixed gas flow rate F these values depend sensitively on the oxygen partial pressure p_{O_2} and the sample temperature T. In the experimental macroscopic phase diagrams these transitions between macroscopic stable steady states of high and low reactivity provide the boundary lines separating the regions in which the system exhibits monostable and bistable behavior.

For *higher pressures* CO oxidation on Pd(110) exhibits an oscillatory region, in which macroscopic temporal oscillations in the reaction rate were observed.[5] By appropriate adjustment of external control parameters it was possible to reproducibly move the system for higher pressures into the oscillatory region, and for lower pressures into the bistable region with stationary high or low reactivity. The experimentally obtained lines separating the two monostable regions

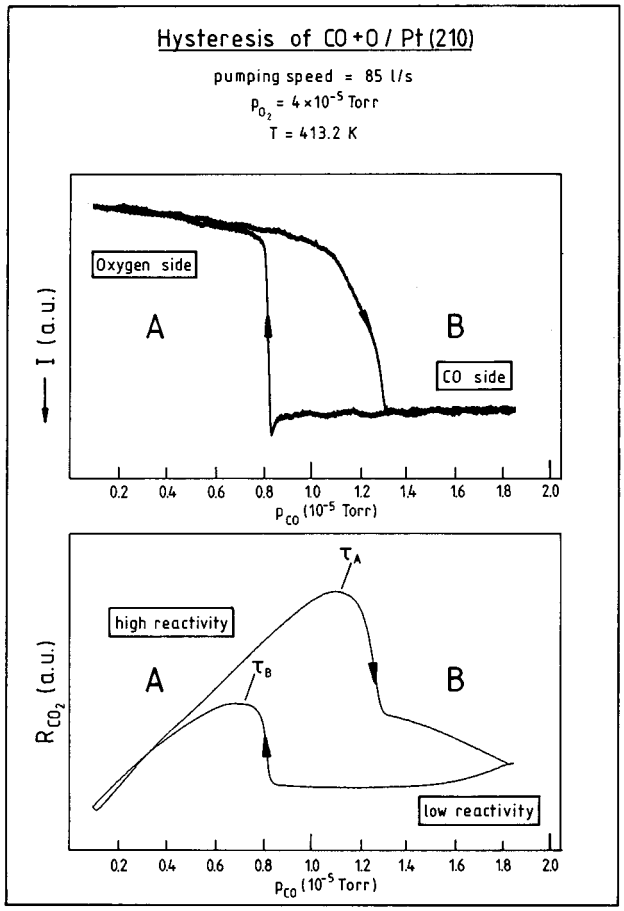

FIG. 1. Macroscopic hysteresis during CO oxidation on Pt(210) can be observed by monitoring the photocurrent measured with the photoelectron emission microscope (upper part) as well as the macroscopic reaction rate (lower part). The surface is covered either with oxygen (high reactivity) or with CO (low reactivity). In reaction rate measurements the transition points τ_A and τ_B are assigned to the experimentally well-defined maximum of the reaction rate.

from the bistable and oscillatory regions approach with increasing pressure, until they cross over, whereupon oscillations occur.

In the following we present detailed experimental data which allow the construction of the kinetic phase diagram for CO oxidation on Pt(210) based on the width of the hysteresis and the observed oscillations at different values of the external control parameters. Some useful general definitions introduced in the previous paper[5] are repeated here for convenience.

1. Hysteresis during CO oxidation

Figure 1 shows an example of hysteresis on a fairly large (51 mm^2) Pt single crystal with (210) orientation. The reactivity as a function of CO partial pressure for fixed flow rate F (85 ℓ/s, also termed pumping speed), oxygen pressure (4×10^{-5} Torr) and sample temperature (413.2 K) was monitored in two independent ways. The first method follows the hysteresis directly as CO_2 partial pressure with a mass spectrometer; the resulting *clockwise hysteresis* is shown at the bottom of Fig. 1. The reactivity was also monitored simultaneously with the photoelectron emission microscope as a CO-pressure-dependent photocurrent, i.e., the image intensity. This measurement is illustrated at the top of Fig. 1. Note that the photocurrent (vertical) axis has negative orientation, the same as often used in measurements of the work function change $\Delta\Phi$. Since the work function of the oxygen-covered Pt(210) surface is higher (lower photocurrent, darker PEEM image) than that of the CO-covered one, this measurement also provides information about the predominant overall surface coverage. The total circular surface area sampled by the microscope was $\approx$380 μm in diameter. The curve shown in Fig. 1 was obtained by digital addition of the intensities of several recorded PEEM images.

For increasing CO pressure ($dp_{CO}/dt>0$) we observe (top part of Fig. 1) a rather abrupt increase of the photocurrent (decrease of the work function) around $p_{CO}=1.2$–1.3×10^{-5} Torr as the surface becomes covered with CO. The reaction rate measurement indicates that this poisoning of the surface is accompanied by a transition to the *macroscopic stable steady state of low reactivity* (also denoted as *CO side*). On the way back ($dp_{CO}/dt<0$) a more abrupt decrease of the photocurrent occurs around 8×10^{-6} Torr, indicative of the surface being covered with oxygen. After this transition the reaction is in the *macroscopic stable steady state of high reactivity (oxygen side)*. For CO pressures below 8×10^{-6} Torr the reaction lies in *monostable region A*, for CO pressures above 1.3×10^{-5} Torr in *monostable region B* and between these two CO pressures in the *experimental bistable region.*

The transition points between the two stable steady states are denoted in Fig. 1 as τ_A and τ_B. In general we define τ as a point of transition between two qualitatively different states of the system. While an external control parameter is changing, the macroscopic stable steady state of high reactivity (low reactivity) originating from monostable region $A(B)$ will loose its stability at the point τ_A (τ_B).

According to Fig. 1, for low CO pressures $p_{CO}<\tau_B(F,p_{O_2},T,\beta)$ the system remains in monostable region A, which is characterized by an almost completely oxygen-covered surface with high reactivity. High CO pressures $p_{CO}>\tau_A(F,p_{O_2},T,\beta)$, on the other hand, move the system into monostable region B which represents a completely CO-covered (poisoned) Pt(210) surface with low reactivity. The bistable region is located between τ_A and τ_B.

For *hysteresis*, τ_A indicates the transition point between the macroscopic stable steady state of high reactivity and the stable steady state of low reactivity (from oxygen side to CO side), while τ_B marks the reverse transition. The observed hysteresis in Fig. 1 is *clockwise* with respect to the CO_2 production rate. Note that $\tau_A>\tau_B$ for a clockwise hysteresis. We obtain the same hysteresis in the macroscopic reaction rate *and* the coverage state of the sample, underlining again the intimate internal connection between overall reactivity and surface chemistry.

2. Time dependence of the hysteresis

An important aspect to consider is the *time dependence* of the hysteresis: the form (width and direction) of the hysteresis loop may change depending on the scanning rate β or may disappear entirely, as predicted in model simulations.[21] Even though it may show time dependence experimentally, a *true hysteresis* is defined by the fact that the region between τ_A and τ_B represents an experimental bistable region ($\tau_A > \tau_B$). To resolve this problem one must, in principle, observe the clockwise hysteresis (Fig. 1) at a virtually negligible scanning rate, so that the system is at all times arbitrarily close to the macroscopic stable steady state. To this end we have performed a series of experiments at constant oxygen partial pressure and temperature in which the scanning rate of the CO partial pressure dp_{CO}/dt was systematically varied. The result of these measurements is shown in Fig. 2, which consists of a series of four scanning cycles performed with $p_{O_2}=4\times10^{-6}$ Torr (left-hand side) and $p_{O_2}=4\times10^{-5}$ Torr (right-hand side). Within each series the time for a half-cycle (upwards or downwards) was varied between 5 min and 8 h, as indicated on each measurement. For high scanning rates a pronounced time dependence is indeed observed. However, for $p_{O_2}=4\times10^{-6}$ Torr the time dependence is very weak for low scanning rates, and an extrapolation of the respective widths of the hysteresis (shown in Fig. 3) suggests that a clockwise hysteresis remains as the scanning rate of the CO pressure approaches values around 10^{-10} to 10^{-11} Torr/s. An inspection of the right-hand side of Fig. 2 and the upper part of Fig. 3 reveals a major difficulty with the aforementioned straightforward way of experimentally determining the branches of the hysteresis (experimental bistable region): Particularly at higher oxygen partial pressures the first impression of a clockwise hysteresis ($\tau_A > \tau_B$) may be utterly misleading—if the scanning rate is sufficiently low a crossing of the two branches occurs, showing that a counterclockwise hysteresis ($\tau_A < \tau_B$) is actually characteristic for the reactivity state of the system.

3. Macroscopic cross-shaped phase diagram

The hysteresis measurements discussed above together with additional measurements at higher oxygen pressures allow us to map the regions of monostable, bistable, and oscillatory behavior for CO oxidation on Pt(210) in the macroscopic isothermal phase diagram shown in Fig. 4. For low oxygen pressures the CO pressure values at τ_A and τ_B obtained for the lowest scanning rate dp_{CO}/dt are depicted as unfilled triangles in this diagram. For an oxygen pressure of 4×10^{-7} Torr and 4×10^{-6} Torr the clockwise hysteresis with $\tau_A > \tau_B$ also remains for very slow scans, indicating the existence of an experimental bistable region. At 4×10^{-5} Torr a counterclockwise hysteresis is obtained for very slow scans. Experiments on Pd(110) show[5,33] that after a crossing of the hysteresis even slower scan leads to the appearance of macroscopic temporal oscillations. According to this experimental observation we regard the crossing of the hysteresis as an indication of the existence of a region with macroscopic temporal oscillatory behavior.

For *macroscopic temporal oscillations* the points τ_A and τ_B denote the boundary of the oscillatory region, according to our general definition of τ. In contrast to the clockwise hysteresis, $\tau_A < \tau_B$ for macroscopic temporal oscillations. For example, if the system originates from monostable region B and the CO pressure is decreased, macroscopic temporal oscillations are first observed at $p_{CO}=\tau_B(F,p_{O_2},T)$. With further decrease of the CO pressure, the macroscopic temporal oscillations persist as long as $p_{CO} > \tau_A(F,p_{O_2},T)$.

At higher pressures ($p_{O_2} \geqslant 4\times10^{-4}$ Torr) a less time-consuming experimental method was used to determine the points τ_A and τ_B (filled triangles). At constant oxygen pressure the CO pressure was varied in a stepwise fashion (3–5 min between each step) and the highest (τ_B) and lowest (τ_A) values of p_{CO} for which oscillatory behavior of the macroscopic reaction rate is observed were used. Ehsasi *et al.*[32] have characterized the macroscopic temporal oscillations on Pt(210) with CO_2 reaction rate measurements. It is shown (Fig. 7 in Ref. 32) that macroscopic temporal oscillations appeared which lasted at least 24 h. The observed macroscopic temporal oscillations are quite similar to the ones found in our work. A single cycle is reproduced in Fig. 9; the oscillations clearly appeared also while the data point at $p_{O_2} \geqslant 4\times10^{-4}$ shown in Fig. 4 was taken.

By plotting the points τ_A and τ_B for different oxygen pressures at a constant temperature, the monostable, bistable, and oscillatory regions are characterized in the macroscopic isothermal phase diagram (Fig. 4). Due to its characteristic shape this diagram is also termed *cross-shaped phase diagram*. For the investigated constant temperature of 413.2 K the crossing point is located at $p_{CO}\approx5\times10^{-6}$ Torr and $p_{O_2}\approx2\times10^{-5}$ Torr.

Since the cross-shaped phase diagram is discussed extensively in a preceding paper dealing with CO oxidation on Pd(110) (Ref. 5) we only draw attention here to an important and remarkable difference in the behavior observed for CO oxidation on Pt(210) as compared to Pd(110). While on Pd(110) all processes (transitions between steady states, oscillations) occur on a short time scale (several seconds to a few minutes) the respective phenomena appear to be greatly retarded on Pt(210). This accounts for the relative difficulty in the determination of the (time-independent) isothermal phase diagram for Pt(210) and the use of two different experimental procedures for the two systems.

B. Pattern formation in CO oxidation on Pt(210)

The photoelectron emission microscope allows a direct observation of the lateral distribution of surface species during the reaction on a mesoscopic scale for pressures below 7×10^{-3} Torr. Since oscillations on Pt(210) appear at lower pressures than on Pd(110), it was possible to investigate the formation of spatiotemporal patterns in the hysteresis and oscillatory regions over an extended parameter regime only on the Pt(210) surface. In earlier investigations on Pt(210) examples of temporal[32] and spatiotemporal oscillations[34,35] have been studied for single sets of external control param-

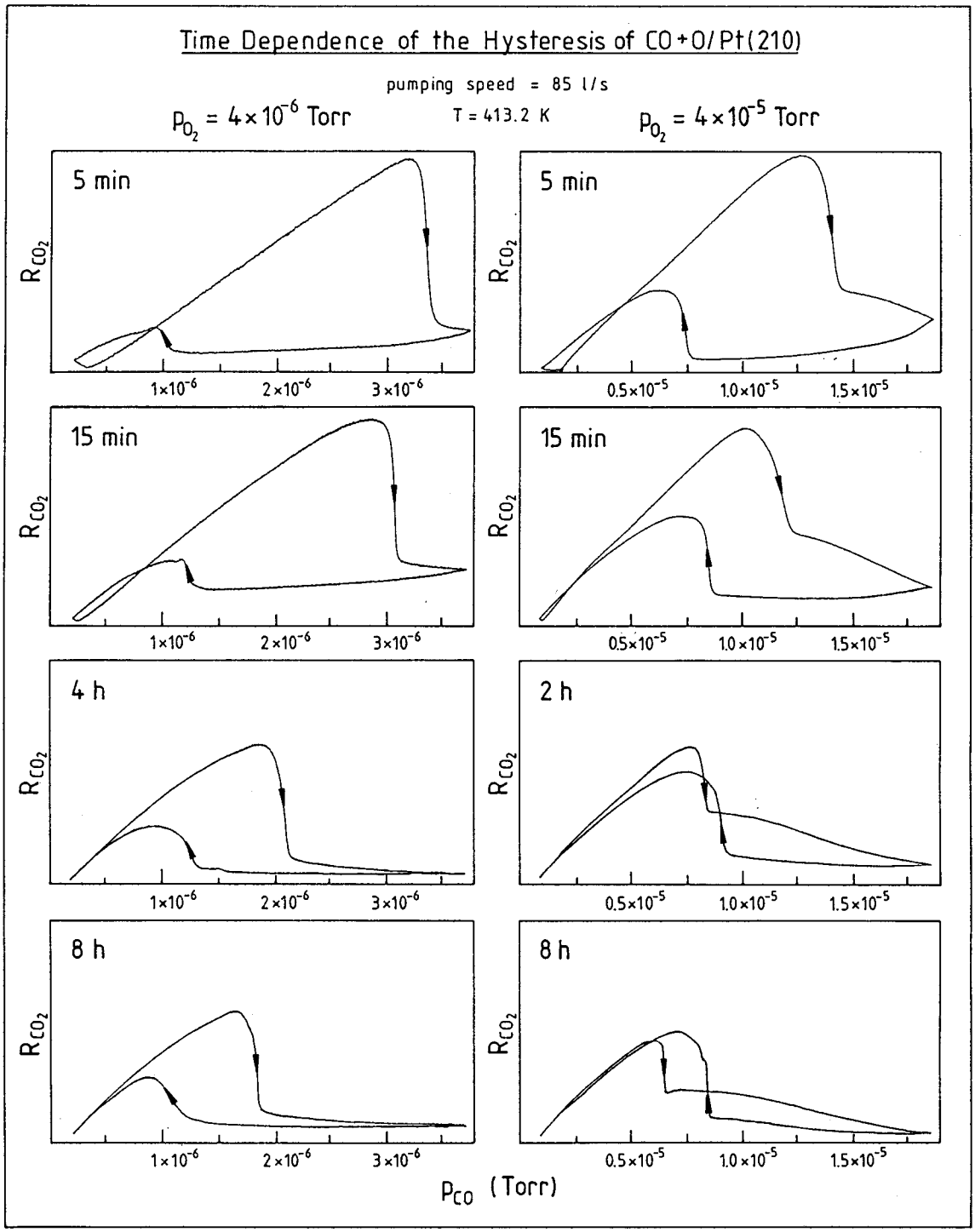

FIG. 2. A systematic variation of the scanning speed of the external control parameter (here the CO pressure) shows that a clockwise hysteresis is obtained for a very low scanning rate at an oxygen pressure of 4×10^{-6} Torr, while similar measurements at 4×10^{-5} Torr yield a counterclockwise hysteresis. Very slow macroscopic temporal oscillations should be possible at 4×10^{-5} Torr, as experiments for Pd(110) show.

eters. Whereas Sander *et al.*[34] found only irregular patterns on the (210) orientation of a cylindrical Pt single crystal, a rich scenario of different spatiotemporal oscillations like target patterns and spirals were observed on a flat Pt(210) surface.[35]

In this section we present results for five different constant oxygen pressures. According to the macroscopic isothermal phase diagram (Fig. 4) measurements presented in Figs. 5 and 6 correspond to external control parameters below the crossing point (hysteresis region), while the conditions in Figs. 7, 8, and 9 are located in the oscillatory region. These experiments clearly demonstrate the different patterns found in the hysteresis and oscillatory regions of the cross-shaped phase diagram.

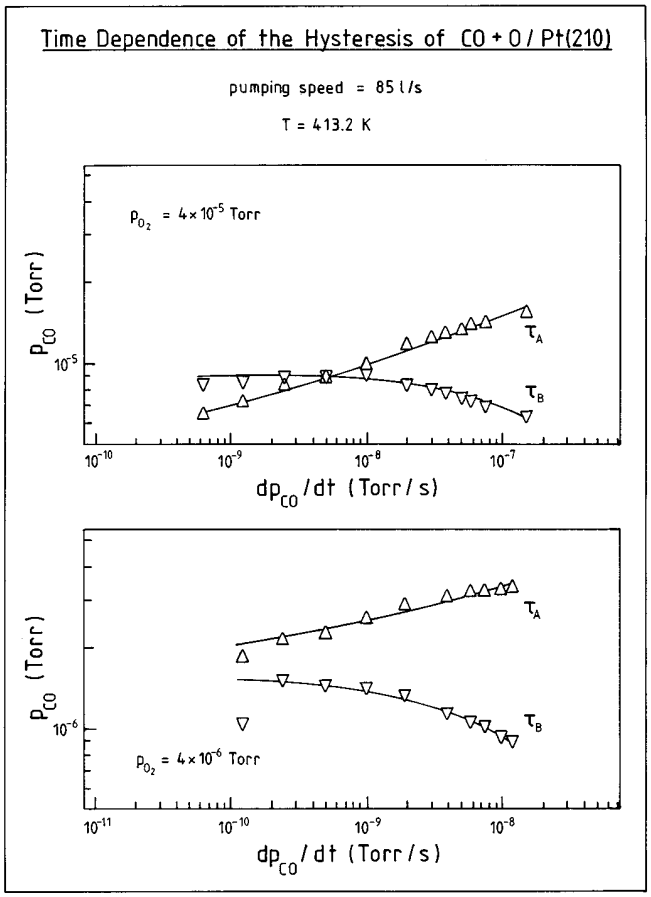

FIG. 3. An evaluation of the measurements shown in Fig. 2 clearly shows how the lines made up of the transition points τ_A and τ_B approach and cross each other with decreasing CO pressure scanning speed at an oxygen pressure of 4×10^{-5} Torr, while at 4×10^{-6} Torr these lines do not meet.

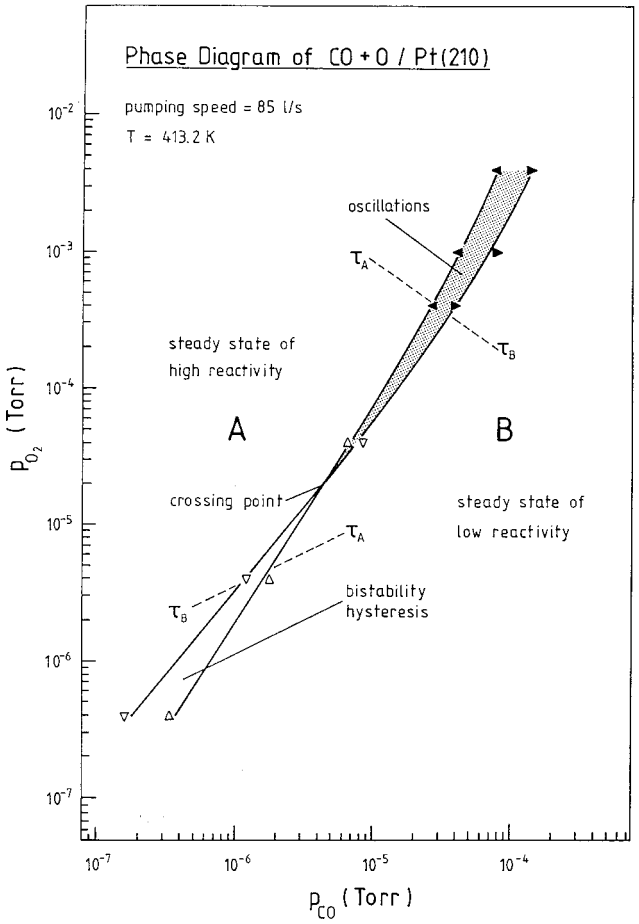

FIG. 4. The experimental isothermal phase diagram shows the bistable region at lower pressures and the oscillatory region at higher pressures. In the monostable region *A* the system is in the macroscopic stable steady state of high reactivity and in the monostable region *B* in the macroscopic stable steady state of low reactivity.

It is important to note that the mesoscopic cross-shaped phase diagram (Sec. III A) was obtained by *variation* of the CO pressure, while the patterns shown in this section were investigated at *constant* control parameters. To clarify how the patterns connect to the phase diagram we give further information about the patterns that appear during CO pressure variation in Figs. 2 and 3.

The variation of CO pressure at various constant oxygen pressures in the range 4×10^{-7} to 4×10^{-5} Torr shows that spatiotemporal patterns are formed during the transition between the different states of the system at both high and low scanning speeds. With decreasing scanning speed the patterns shown in the hysteresis experiments in Figs. 2 and 3 change continuously and come to resemble more and more the patterns shown below obtained at constant external control parameters. However, even for very low experimental scanning speeds the patterns can only be formed in a short time interval. Only at constant external control parameters is there enough time for their full development (Figs. 5–9).

Note that the constant CO pressures chosen for the PEEM experiments presented below lie in close proximity to the lines formed by the transition points τ_A and τ_B (Fig. 4). During a change toward a CO pressure that lies farther away from these lines of transition (far into the monostable region *A* or *B*), the observed transitions resemble those obtained at higher scanning speeds. Many smaller islands form in addition to the larger ones, and the previously formed rudimentary target patterns are quickly transformed into islands. Thus the spatiotemporal patterns presented below in this section reflect the behavior of the system in the neighborhood of the lines formed by the transition points τ_A and τ_B or in the interior of the oscillatory region of the cross-shaped phase diagram. (A detailed description of the experiments with PEEM images obtained at high and low scanning speeds is the subject of a separate publication.) We emphasize that for Pt(210) no oscillations have as of yet been observed with a *homogeneous* change of adsorbate coverage; patterns have always been found on the surface.

Before looking at the results in detail, we recall the correlation between the surface work function and the brightness of the PEEM image mentioned in Sec. II. Areas with high electron work function yield low photocurrent, which, in turn, leads to dark regions in the PEEM image. Since the work function increase on platinum is higher for a saturated

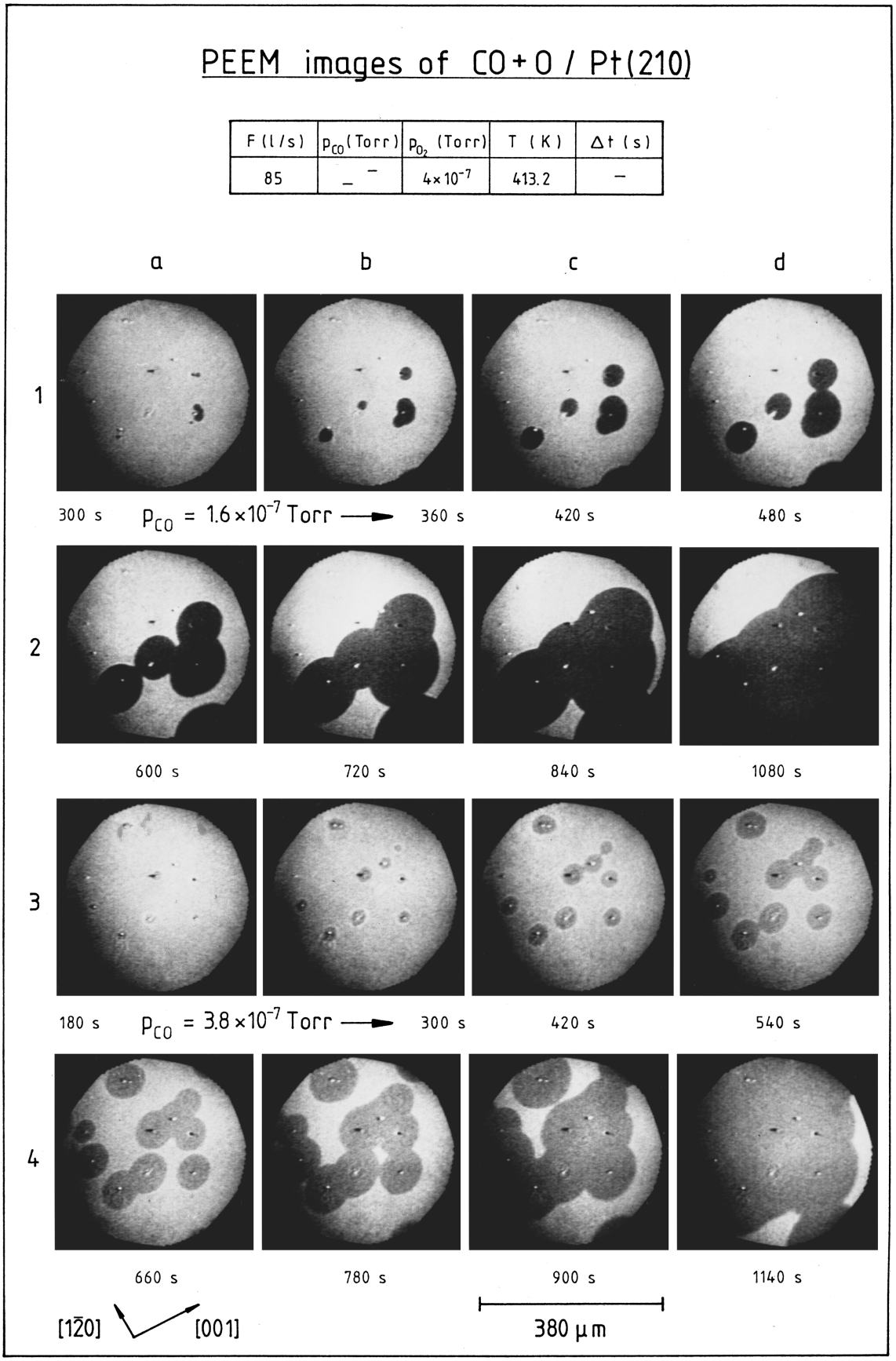

FIG. 5. In the hysteresis region far below the crossing point, oxygen islands (rows 1 and 2) and CO islands (rows 3 and 4) can be observed during the transition between the respective macroscopic stable steady states. The external control parameters are indicated in the upper part of this and the following figures. At the time $t=0$ the pressure jump is made to the indicated value.

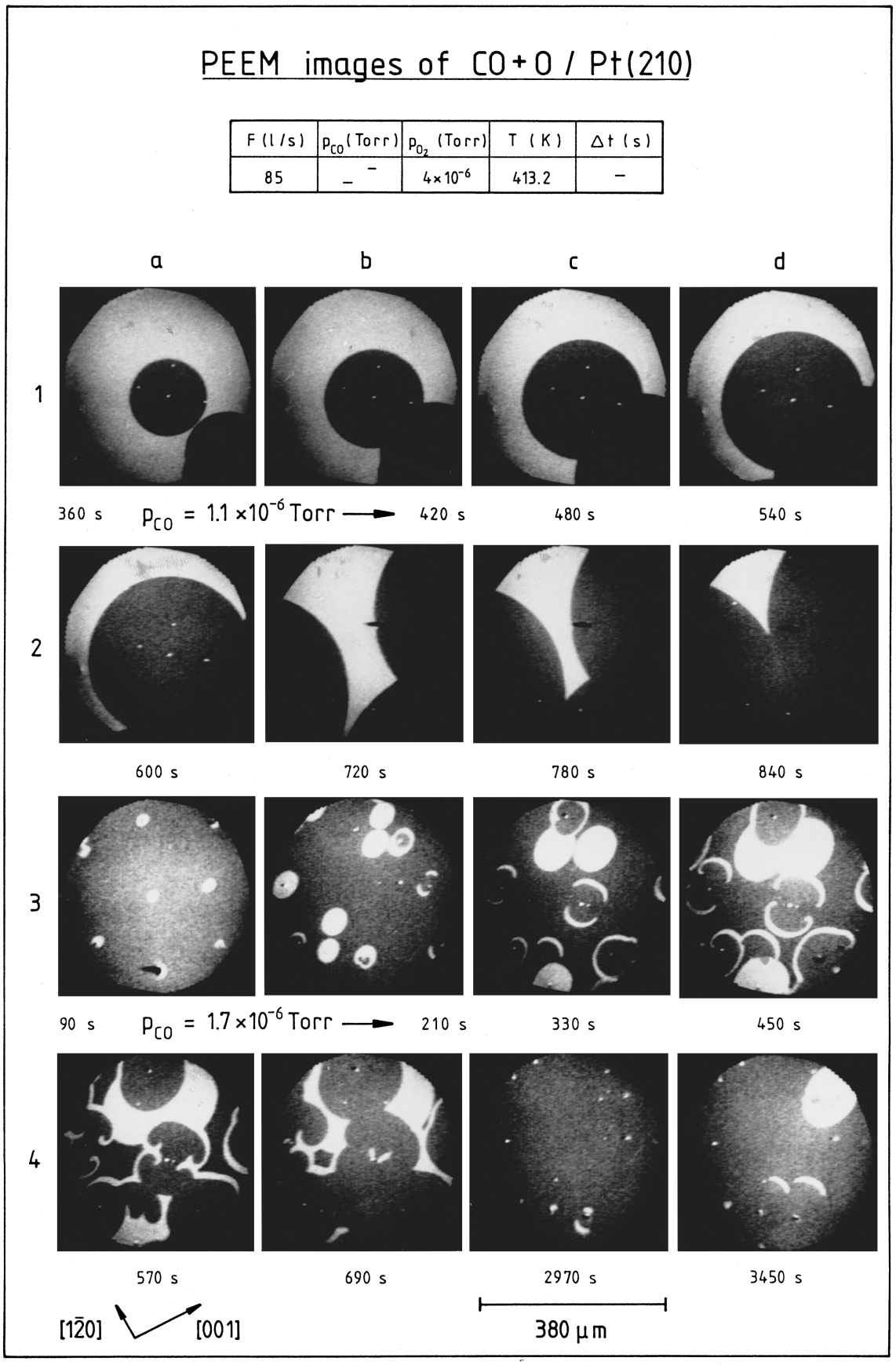

FIG. 6. Immediately below the crossing point, oxygen islands (dark, rows 1 and 2) and CO islands (bright), as well as CO waves (rows 3 and 4) appear.

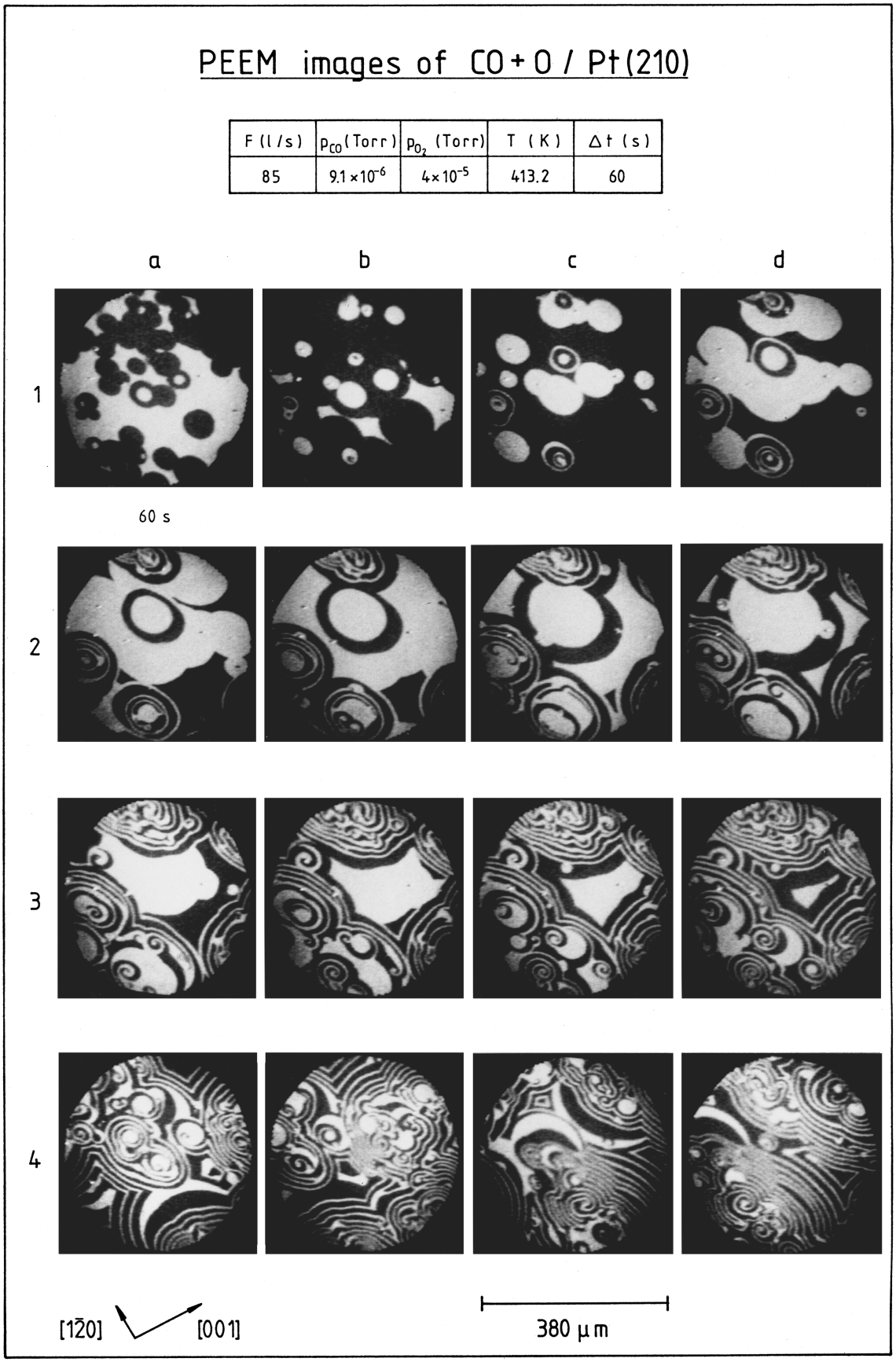

FIG. 7. In the oscillatory region above the crossing point, complicated spatiotemporal patterns form on the surface. The time interval Δt between successive images is 60 s.

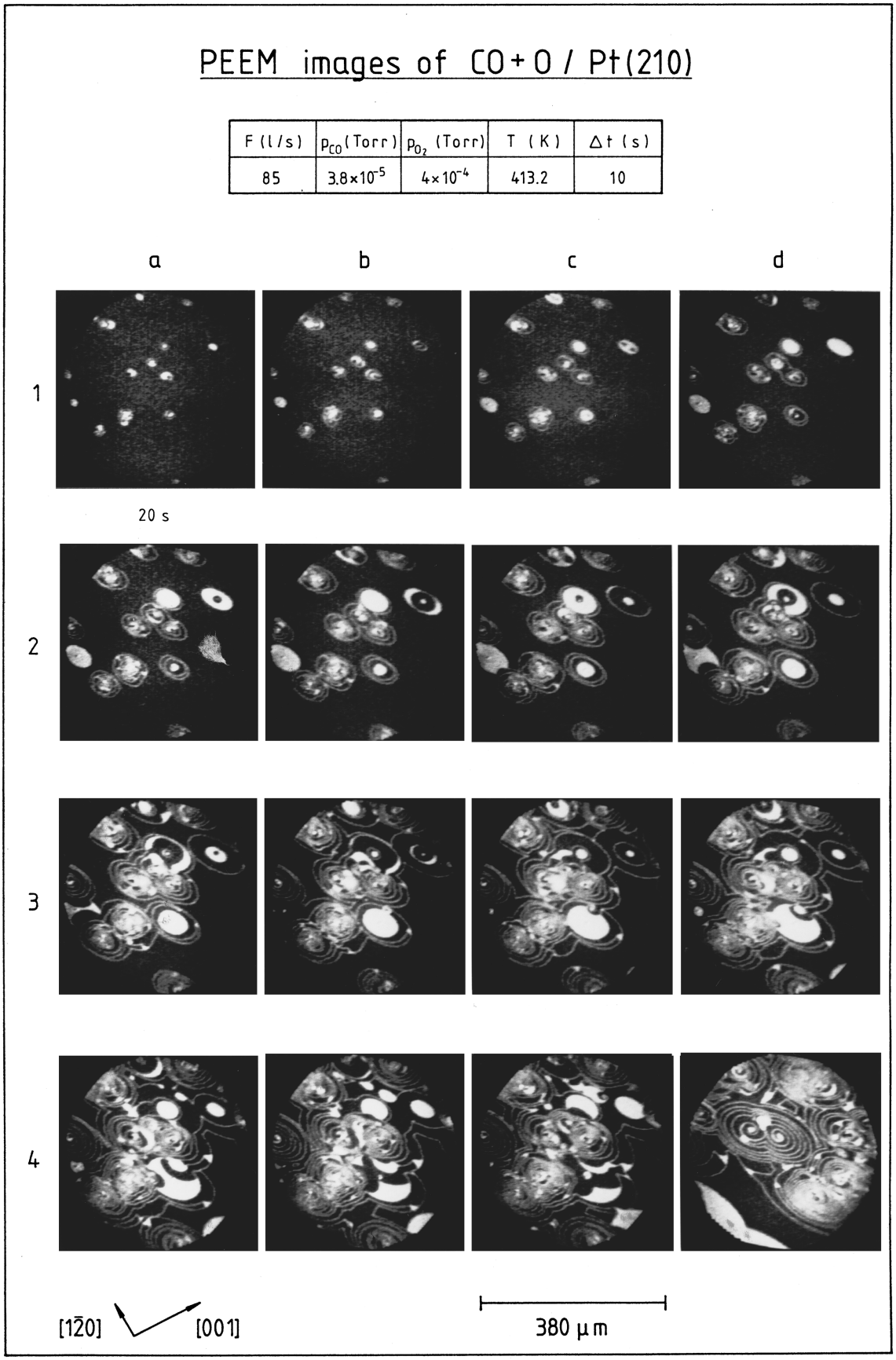

FIG. 8. With increasing pressure farther from the crossing point, the movement of the reaction/diffusion fronts becomes more rapid and their width becomes narrower. The local oscillator in the center of the target pattern also oscillates more rapidly.

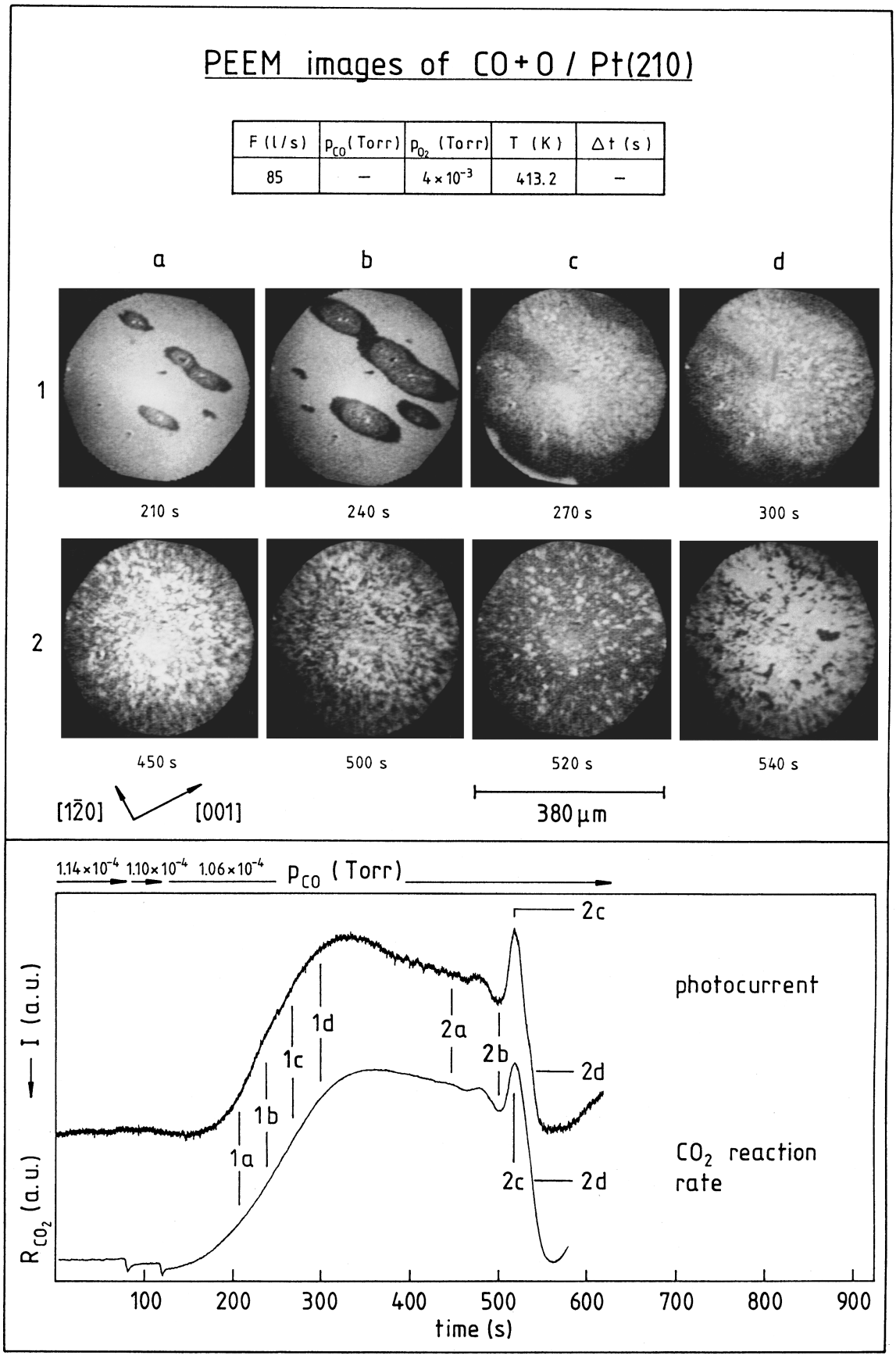

FIG. 9. At a high oxygen pressure far above the crossing point, adsorbate patterns on the surface become diffuse in a short time interval (top part). The macroscopic reaction rate (bottom part) is clearly correlated with the photocurrent from the surface area shown above. One oscillation period is shown.

oxygen-covered area than for a CO-covered one, areas covered with *oxygen* always appear *dark* in the PEEM image. CO-covered regions are bright if surrounded by oxygen, which is usually the case for those pressures at which high local coverages are attained (above $\approx 1\times10^{-6}$ Torr). They can, however, appear relatively dark if surrounded by an uncovered surface. An example for this rare exception is given in Figs. 5.3 and 5.4.

1. Pattern formation in the hysteresis region

The images in Fig. 5 were obtained for an oxygen pressure of 4×10^{-7} Torr, which is located *far below the crossing point* in the hysteresis region of the macroscopic isothermal phase diagram (the remaining external control parameters, the time after the pressure jump and the time interval Δt between successive images are given in the figures). This figure displays two series of PEEM images, each series obtained at a different CO pressure. The upper two rows (Figs. 5.1 and 5.2) display the growing of oxygen islands, and the lower two rows (Figs. 5.3 and 5.4) show CO islands growing.

These series were obtained with the following procedure: First a CO pressure is established ($p_{CO_2}=4\times10^{-7}$ Torr) at which the surface is completely covered with CO or oxygen. Next a pressure jump is made by quickly adjusting the pressure controller to a CO pressure value at which the growth of CO islands (jump to higher p_{CO}) or oxygen islands (jump to lower p_{CO}) is possible. It takes 5–10 s for the chamber pressure to adjust to the new value set by the controller. The external control parameters are kept constant after this pressure jump. The time at which the electronic regulation to the new CO pressure begins is defined as the beginning of the measurement ($t=0$). The small shadow in the lower left corner of each image is an experimental artifact.

The growth of oxygen islands can be seen in Figs. 5.1 and 5.2 at a CO pressure of 1.6×10^{-7} Torr. The first image [Fig. 5.1(a)] shows the situation 300 s after the pressure jump. There are clearly some mesoscopic defects on the surface with a diameter between 1 and 10 μm. Small oxygen islands are visible at two defects on the right-hand side of the image. In the next picture [Fig. 5.1(b)] two more oxygen islands have formed on the surface. An oxygen island grows in the following sequence of images from the lower right of the surrounding surface into the imaged area. This sequence shows that the islands grow with time until the whole surface is completely covered with oxygen. The reaction is now in the macroscopic stable steady state of high reactivity (oxygen side).

The second series (Figs. 5.3 and 5.4) at $p_{CO}=3.8\times10^{-7}$ Torr shows the same surface area. In contrast to oxygen islands, CO islands are formed at almost every mesoscopic defect visible on the surface. All CO islands in the observed area are formed in a narrow time interval with similar diameter during the growth. At first a small bright ring is visible around the islands, which may be attributed to surrounding lower coverages of CO and/or oxygen. The CO islands spread with time over the whole Pt(210) surface in the same manner as the oxygen islands. In the end the surface is completely covered with CO and the reaction is in the macroscopic stable steady state of low reactivity (CO side). Both series demonstrate that under these conditions the phase transition between the two macroscopic stable steady states proceeds via a growth of several large islands.

Figure 6 presents images obtained at an oxygen pressure of 4×10^{-6} Torr. This oxygen pressure is *just below the crossing point* of the macroscopic cross-shaped phase diagram in Fig. 4, but still in the hysteresis region. The experimental procedure is the same as described above for Fig. 5. The transition from the macroscopic stable steady state of low reactivity to the macroscopic stable steady state of high reactivity again proceeds via oxygen island growth (Figs. 6.1 and 6.2). In this experiment, however, only a single oxygen island is formed in the observed area. Remarkably, *no oxygen islands develop at the other five visible mesoscopic defects*. The shape of the single oxygen island is perfectly circular. A more complicated situation is obtained in Figs. 6.3 and 6.4, where the surface is first covered with oxygen and then a pressure jump is made to a CO pressure at which CO islands can grow. Note that different crystal positions are depicted in Figs. 6.3(a)–6.3(c), showing that the same processes occur on the entire surface. Again a CO island is formed at almost every defect with a diameter between 1 and 10 μm. After a certain time interval an oxygen island grows inside some of the CO islands, leaving only circular CO waves behind. These waves break up into two semicircles whose ends start to curve inward [Figs. 6.3(c) and 6.3(d)]. If the four ends of these opposing waves had not mutually annihilated each other, they would have formed spirals [Figs. 6.4(a) and 6.4(b)], as discussed in Ref. 36 and shown in simulations.[37] In the following images one can see how these patterns slowly disappear [Figs. 6.4(b) and 6.4(c)]. Finally the surface is almost completely covered with oxygen again [Fig. 6.4(c)]. After several minutes, however, a similar sequence begins to develop [Fig. 6.4(d)]; a stable CO-covered surface was not observed under these conditions. Therefore it seems that at this oxygen pressure a small region exists in the neighborhood of line τ_A in Fig. 4, in which spatiotemporal oscillations are possible.

2. Pattern formation in the oscillatory region

According to the macroscopic cross-shaped phase diagram a further increase in oxygen pressure to 4×10^{-5} Torr (Fig. 7) leads to conditions *immediately above the crossing point*, where oscillations can occur. The time interval Δt between the pictures in the following sequence (Figs. 7.1–7.4) is 60 s. At the start of the sequence the surface was almost completely covered with CO. 60 s after the jump from a CO pressure in monostable region *B* down to $p_{CO}=9.1\times10^{-6}$ Torr [Fig. 7.1(a)], many oxygen islands arise at mesoscopic defects on the CO-covered surface. CO islands again develop at these defects inside the oxygen-covered regions, resulting in the development of a target pattern. This process leads to complicated patterns such as tar-

get patterns and spirals in the following images (Figs. 7.2 and 7.3). In the lower part of these images one end of a wave begins to curl inward, thereby forming a one-armed spiral. On the left side another wave is visible, each end of which curls up in opposite directions (Fig. 7.2). In Fig. 7.4 the crystal was moved to show that the whole surface is covered with these complicated patterns and no extended CO islands remain.

Figure 8 shows PEEM images at an oxygen pressure of 4×10^{-4} Torr, which is located in the oscillatory region *well above the crossing point* in Fig. 4. The same surface area is shown as in Fig. 5. Only 20 s after the CO pressure change, CO islands and target patterns develop at the defects. At these same defects CO islands had appeared in Fig. 5 at lower oxygen pressures. The patterns developing in Fig. 8 spread over the whole surface. At the upper right of the images a target patterns with significantly longer period than that of the other patterns takes shape. The last image [Fig. 8.4(d)] shows two neighboring one-armed spirals.

We emphasize that the images discussed above (Figs. 6.3, 6.4, 7, and 8) show the development of patterns *immediately* after a CO pressure jump. In the frame of the present work we cannot go into the detailed *further* temporal development of these patterns. It may, for example, be possible that after a sufficiently long time interval a transition to the CO side occurs, succeeding the measurements presented in Figs. 6.3 and 6.4. Figures 7 and 8 show only the beginning of the temporal evolution of the patterns which subsequently become increasingly complex (not shown in Figs. 7 and 8), leading finally to a completely CO-covered surface. The development of spatiotemporal oscillations can thus go hand in hand with very slow (temporal) oscillations in the reaction rate. Therefore temporal as well as spatiotemporal oscillations can exist, which is indicative of coupling via the gas phase and via reaction/diffusion fronts. It is not yet clear, however, if this behavior can in fact be attributed to the superposition of spatiotemporal oscillations and macroscopic temporal oscillations via gas phase coupling or an internal feedback. Another experimental problem with might be connected with the present observation of the further temporal pattern evolution concerns the change in the probe position with reference to the PEEM aperture (performed after the measurements shown in the images of Figs. 7 and 8), by virtue of which the local CO pressure above the sample is slightly altered. In order to observe either temporal or spatiotemporal oscillations alone, significantly longer measurement times would be required, however. To obtain an idea of how temporal reaction rate oscillations go hand in hand with spatiotemporal oscillation we show the correlation between PEEM images and the photocurrent measured at an elevated oxygen pressure.

Figure 9 shows such a measurement at an oxygen pressure of 4×10^{-3} Torr. This figure is divided into two parts, the upper part showing a series of PEEM images, the lower part displaying the integrated photocurrent simultaneously derived from the area (380 μm diam) observed by the photoelectron emission microscope, along with the overall CO_2 production rate measured macroscopically with the mass spectrometer. The lower part of the figure is accompanied by references to the corresponding PEEM pictures in the upper part.

The local photocurrent is correlated with the macroscopic reaction rate in every detail during the measurement. With other external control parameters kept constant, the CO pressure was decreased slightly two times in order to trigger the oscillatory cycle, which begins after the second small pressure decrease. Again at almost every observable surface defect small oxygen islands develop [Fig. 9.1(a)]. Due to the high reactivity of the oxygen-covered surface, the overall detectable CO_2 production rate starts to increase. After a certain time a CO adlayer forms inside some of these islands [Figs. 9.1(a) and 9.1(b)]. The formed oxygen waves unite and finally disappear with increasing size [Figs. 9.1(b) and 9.1(c)]. At this stage the surface is *left covered with small irregular CO and oxygen islands*. Now the reactivity decreases and the borders of the small islands become sharper [Fig. 9.2(a)]. Next fast oscillations with small amplitudes develop on the high reactive branch of the slow relaxation-type oscillatory cycle (oscillation between an almost completely CO-covered and oxygen-covered surface state). It is evident that at the following relative minimum [Fig. 9.2(b)] and maximum of the reactivity [Fig. 9.2(c)] *both CO and oxygen are present on the surface*. During the oscillation cycle CO and oxygen exist in small islands on the surface. After approximately 520 s the oscillatory cycle has reached its maximum reactivity with high oxygen coverage, whereupon the surface shows a transition to the CO side, being finally poisoned by CO and showing low reactivity [Fig. 9.2(d)]. The succeeding oscillatory cycles (not shown in Fig. 9) behave in a similar manner.

The slow relaxation-type oscillatory cycle discussed here was also observed by Ehsasi *et al.* on a Pt(210) single crystal.[32] About 2 h after the observation of this cycle very regular, slow relaxation-type oscillations with a period between 200 and 300 s were obtained. Significantly faster macroscopic temporal oscillations have seldom been observed on this crystal. PEEM images of such rare fast macroscopic temporal oscillations[19] show patterns similar to those of Fig. 9.2.

3. Properties of fronts and local oscillators

Spatiotemporal oscillations propagate from the local oscillators, which are usually bound to defects. This makes possible an analysis of the velocity of the reaction/diffusion fronts as well as the period of the local oscillators. Since a certain anisotropy exists in the front motion, the front velocity is always calculated in the four o'clock direction in the images, which is the direction of greatest front velocity for higher pressures. Table I shows that the velocity of the reaction/diffusion fronts increases with oxygen pressure, whereas the period of local oscillators decreases with pressure. Furthermore it can be seen in Figs. 7 and 8 that the width of the waves also increases with oxygen pressure. Since the patterns are very diffuse at 4×10^{-3} Torr, the period of the local oscillator cannot be determined. It should be

TABLE I. Dependence of front velocity and period of local oscillators on oxygen pressure.

Oxygen pressure (Torr)	Period of local oscillators Front velocity (μm/s)		(s)
4×10^{-7}	CO island:	0.065	(no oscillations)
	oxygen island:	0.13	
4×10^{-6}	CO island:	0.13	(no oscillations)
	oxygen island:	0.33	
4×10^{-5}	0.28		65
4×10^{-4}	0.7		17
4×10^{-3}	1.2		-

noted that the CO pressure also has an effect on the front velocity and the period of the local oscillators; the values given in the table therefore represent only order-of-magnitude values for the respective oxygen pressure.

IV. DISCUSSION

We emphasize here the correlation of the patterns observed on the surface with the experimental macroscopic cross-shaped phase diagram and propose experimentally well-founded requirements for mathematical simulations. The importance of the phase diagram in reference to the reaction mechanism will only receive marginal attention, as this has already been discussed in detail in previous work on Pd(110).[5] In addition we discuss the occurrence of macroscopic temporal oscillations and spatiotemporal pattern which are formed during CO oxidation on Pt(210). Finally we compare the patterns found on Pt(210) with those found on other single-crystal surfaces.

A. Construction of the macroscopic isothermal phase diagram

The first part of the section on experimental results showed the measurement procedure used for obtaining the macroscopic isothermal phase diagram for CO oxidation on Pt(210), while the second part presented mesoscopic PEEM images of adsorbate patterns for several oxygen pressures. An important result of this first part is that hysteresis is observed on Pt(210) at lower, and oscillatory behavior at higher pressures, as can be seen in the resulting cross-shaped phase diagram.

For lower pressures just above the crossing point, the oscillatory region was determined by a continuous variation of the CO pressure, showing counterclockwise hysteresis (Fig. 2). The experiments in Figs. 2 and 3 reveal a clockwise hysteresis for fast scans of the CO pressure and a counterclockwise hysteresis for slow scans, indicative of macroscopic temporal oscillations at very low scanning rate. Similar experiments for Pd(110) show that after such a hysteresis crossing, macroscopic temporal oscillations appear for much slower scans.[5,33] The experimental result in Figs. 2 and 3 thus makes plausible the hypothesis that macroscopic temporal oscillations can already take place under these conditions. An experimental confirmation of a macroscopic oscillatory behavior near the crossing point may be difficult, however, because the oscillatory region is quite narrow and the periods of macroscopic temporal oscillations on Pt(210) will be very long.

Further it was shown that the inherent properties of the examined system must be taken into account during the experimental construction of this phase diagram. An important aspect of CO oxidation on Pt(210) is that temporal processes occur much more slowly on this crystal than on Pt(110) or Pd(110). From Fig. 2 it is evident that hysteresis can be observed, at least in the oscillatory region, if the external control parameter is varied too rapidly. If measurements were only performed in which the parameter is varied rapidly, a phase diagram would result which would feign a system in which no oscillations occur. This result would clearly have far-reaching consequences for the theoretical construction of the reaction mechanism; although the bistable region is predicted qualitatively by the Langmuir–Hinshelwood mechanism, oscillations are not.

B. Connection between experiments and reaction mechanism

Experiments and model calculations show that the reaction mechanism for an oscillating homogeneous system for which a computed macroscopic cross-shaped phase diagram is found must formally be made up of at least two subsystems.[13,38] One subsystem reflects the bistability of the reaction, and the other is responsible for a slow feedback process. For CO oxidation on single-crystal surfaces the Langmuir–Hinshelwood mechanism describes an inherent bistability; the feedback process necessary for oscillations remains controversial, however. Two prime candidates for the latter process are (1) a change in surface morphology [development of (110) facets and their reconstruction[30]] and (2) an additional oxygen state, like subsurface oxygen, oxide, etc.[19,39]

Mathematical formulations of the reaction mechanism based on the Langmuir–Hinshelwood reaction steps and one of the aforementioned alternative feedback processes yield computed macroscopic kinetic phase diagrams showing reactive regions as a function of external control parameters.[40,41] These simulations show the degree to which the reaction steps and other included assumptions can, in principle, describe the macroscopic catalytic reaction.

Sander *et al.*[30] have discussed a close similarity between the oscillatory mechanisms for Pt(210) and Pt(110) and state:

> *The faceting process is essential for kinetic oscillations on Pt(210) since it produces the (110) terraces on which the CO-induced* $1\times1\rightleftarrows1\times2$ *phase transition can proceed. The* $1\times1\rightleftarrows1\times2$ *phase transition has been shown to be the actual driving force of the oscillations on Pt(210). The oscillation mechanism can thus be described as a two-stage faceting/phase transition mechanism whose elementary steps are the same as in the oscillatory system Pt(110)/CO+*O_2.

This would indicate that simulations performed for Pt(110) should in principle—at least qualitatively—describe the CO oxidation also on Pt(210), which has, however, not

been proved to be the case. Using the reconstruction mechanism, a detailed computed macroscopic isothermal phase diagram was obtained for CO oxidation on Pt(110).[9,40] In this computed cross-shaped phase diagram a bistable region is located at higher pressures and an oscillatory region at lower pressures. In addition, the oscillatory region narrows with increasing pressures. These findings conflict with the obtained experimental cross-shaped phase diagram for Pt(210) (Fig. 4). The reconstruction mechanism therefore cannot reproduce the salient features of the phase diagram for Pt(210) discussed here, at least not as long as further simulations could revert the orientation of the bistable and oscillatory region in the isothermal phase diagram.

We have to emphasize here that this disagreement between experimental and computed phase diagram is not a sufficient condition to rule out the reconstruction mechanism as the cause for oscillations on Pt(210). Also for the oscillatory CO oxidation on Pd(110) the computed phase diagram had in the beginning an inverted orientation as the experimental phase diagram. An additional improvement of the subsurface oxygen model by Hartmann *et al.*[42] results in a qualitatively right orientation of the computed cross-shaped phase diagram.

Nevertheless new TDS experiments with oxygen adsorption on Pt(210) from Moldenhauer *et al.*[39] show that additional oxygen binding states are formed at elevated oxygen exposures. These new states could not be saturated up to very large exposures and likely indicate subsurface oxygen species. This species, which has been shown to cause oscillatory behavior of the CO oxidation on Pd(110) could also play a decisive role in the oscillations on Pt(210). It is remarkable in this context that the computed cross-shaped phase diagram obtained for Pd(110) (Ref. 42) on the basis of the subsurface oxygen mechanism exhibits qualitative similarities with the experimental cross-shaped phase diagram for Pt(210). All in all, further investigations are certainly necessary to explore the origin of the kinetic oscillations and the experimental cross-shaped phase diagram for the CO oxidation on Pt(210).

C. Connection between mesoscopic spatiotemporal patterns and (macroscopic) phase diagrams

Additional information about model equations and the reaction mechanism is gained by a comparison of the patterns obtained in the experiments and simulations, respectively. The appearance of specific patterns that depend on external control parameters has been mapped experimentally only twice in the parameter space, namely for the reaction between CO and oxygen on Pt(110) at constant oxygen pressure[8] and for the CO+NO reaction on Pt(100) at a constant NO pressure.[43]

For the case of CO oxidation by oxygen on Pt(110), spirals were found throughout the examined temperature range 380–520 K. For temperatures between approximately 470 and 520 K localized patterns termed solitary oxygen waves were found on the CO side just outside of the spiral region. Another type of behavior termed double metastability

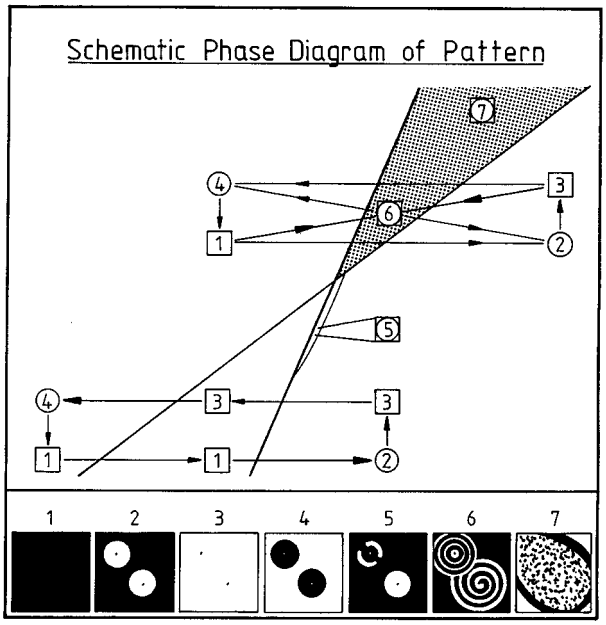

FIG. 10. The schematic cross-shaped phase diagram shows the monostable, bistable, and oscillatory regions and indicates the spatiotemporal patterns that form in them.

was found at temperatures between 380 and 470 K, localized on the oxygen side just outside the spiral region. In this domain islands arise and grow. In the interior of these islands another island made up of the other adsorbate can form at a different defect, thus leading to alternating CO and oxygen *islands*.

The results for CO oxidation on Pt(210) shown here permit, for the first time, the association of various mesoscopic adsorbate patterns with an independently determined experimental macroscopic kinetic phase diagram. Furthermore this macroscopic isothermal phase diagram displays not just a single region of hysteresis or oscillations but both regions connected to each other in one parameter plane. To facilitate an overview over the complex behavior encountered in this system, Fig. 10 outlines the main observations by showing schematically the experimental macroscopic cross-shaped phase diagram of Fig. 4 together with the mesoscopic patterns observed at different oxygen pressures presented separately above in Figs. 5–9.

If the CO pressure is high in relation to the oxygen pressure, then the surface will be completely covered with CO (monostable region B), while low CO pressures lead to a surface predominately covered with oxygen (monostable region A). Below the crossing point (lower pressures) these two monostable states are separated by an experimental bistable region in which the surface is homogeneously covered with CO (Fig. 10.3) or oxygen (Fig. 10.1), depending on the previous conditions. Inside the experimental bistable region no patterns are formed if the external control parameter is changed from values in a monostable region to a value in the experimental bistable region. A change of an external control parameter moving the system from one monostable region to the other leads to CO or oxygen islands forming at

inhomogeneities (defects) and spreading over the whole surface (Fig. 10 sequence 1, 2, 3 and 3, 4, 1). This agrees with the observation of island formation during CO oxidation on Pt(111).[19,20] For that system only monostable and bistable regions were observed, and the transitions between macroscopic stable steady states also occur via island growth. For Pt(111) special prepared islands remain stable inside the experimental bistable region without a motion of the fronts. We emphasize once more that the experimental bistable region is located inside the computed bistable region (assisted nucleation region). Of course one can observe island growth in the rest of the computed bistable region which is, as pointed out above, wider than the experimental bistable region.

Not far below the crossing point a small region appears next to the line formed by the transition points τ_A, in which single waves form together with CO islands (Fig. 10.5). The present measurements do not reveal further detail about the boundaries of this region and its exact location in the neighborhood of the crossing point. At pressures above the crossing point the oscillatory region is located between the monostable regions A and B; here complex spatiotemporal oscillatory patterns such as target patterns and spirals (Fig. 10.6) are encountered. The patterns originate from defects, similar to the formation of islands, but here an adsorbate layer of the other reactant soon forms inside a previously established pattern. Far above the crossing point, finally, many small islandlike patterns are observed (Fig. 10.7).

Over the whole parameter range surveyed no region was found in which oscillations are accompanied by a homogeneous, global change of adsorbate coverage. A change of an external control parameter moving the system from one monostable region to the other leads to CO (Fig. 10 from 1 to 2) or oxygen islands (Fig. 10 from 3 to 4) forming at inhomogeneities (defects) and spreading over the whole surface.

The qualitative observation that simple islands form below the crossing point and complex patterns like spirals and target patterns form above it can be understood as the increasing influence with pressure of a slow-acting feedback process. This process also seems to play an important role in the formation of spatiotemporal oscillations on a mesoscopic scale. Its effect is enhanced at the defects and leads to the appearance of spatiotemporal oscillations, whose various spatial patterns (especially waves, target patterns, and spirals) show regular geometric shapes. Subsequent interaction among these regular patterns then leads with time to diverse irregular patterns.

The results make clear that the macroscopic phase diagram is correlated with the main features of pattern formation on a mesoscopic scale. On a macroscopic scale a proposed reaction mechanism must at least predict hysteresis at lower oxygen pressures and oscillations at higher pressures. Further taking into account mesoscopic spatial adsorbate structures would also include island growth as the process of transition between macroscopic stable steady states (Figs. 5 and 6). In the *experimental* bistable region *no patterns* were observed. In the oscillatory regime complicated spatiotemporal patterns appear, the most striking of which are target patterns and spirals (Figs. 7 and 8). At high oxygen pressures far above the crossing point, small islandlike patterns appear on the surface (Fig. 9). These findings represent a list of phenomena that a proposed reaction mechanism should predict.

D. Comparison of pattern formation with other systems

For model calculations it is important to know wherein the differences and similarities in pattern formation during CO oxidation on Pt(210) and other single-crystal surfaces lie. Evidently the experimental characterization of such systems [CO oxidation on Pt(210) and on other investigated surfaces] is by no means complete, and thus a conclusive discussion of pattern formation is at present not possible. A common feature of the pattern observed on the studied surfaces [Pt(100) (Ref. 44), Pt(110) (Refs. 7, 8), Pt(210) (Ref. 6), and Pd(110) (Ref. 45)] is the formation of waves, which make up such more complex pattern as traveling waves, target pattern, and spirals. Pt(100) is somewhat exempt from this general rule; up to now a spiral-like pattern was observed momentarily in only a few instances on this surface.[44] In most cases islands, target pattern, and spirals propagate from defects on the surface of the single crystals. It is remarkable that spatiotemporal patterns form in great number on Pt(110) and Pt(210), while their observation on Pt(100) and Pd(110) seems to bring on pronounced difficulties, the physicochemical cause of which has remained unclear.

A remarkable and fascinating type of pattern very distinct from all other patterns discussed above was observed on Pt(110).[7] These patterns, known as standing waves, exhibit various structures usually made up of deformed quasirectangular wave trains. Certain segments are offset by a half-period against each other, leading to a diversity of patterns. The oscillatory cycle repeats in time intervals of less than 1s, resembling alternating positive and negative images.

The literature[8,28,43] and the present work show that it is important for a systematic, methodical study of spatiotemporal patterns to characterize these as a function of their external control parameters. Proceeding from such studies it is possible to discuss in more detail the similarities and differences between the various surfaces. By comparing simulations with the experiments it may then be possible to extract characteristic physical parameters which determine certain patterns. Such an effort would yield not only a set of images of surface patterns, but, with their correlation to the control parameters, also a deeper insight into the processes relevant for heterogeneous catalytic reactions.

ACKNOWLEDGMENTS

A.K. and G.G.Y. thank the Max-Planck-Gesellschaft for a fellowship. Support by the Max-Buchner-Forschungsstiftung is also gratefully acknowledged. We also thank Timm Rebitzki for a critical reading of the manuscript and Mohammad Ehsasi for helpful discussions.

[1] G. Nicolis and I. Prigogine, *Self-Organization in Nonequilibrium Systems, From Dissipative Structures to Order through Fluctuations* (Wiley, New York, 1977).
[2] L. F. Razon and R. A. Schmitz, Catal. Rev. Sci. Eng. **28**, 89 (1986).
[3] F. Schüth, B. E. Henry, and L. D. Schmidt, Adv. Catal. **39**, 51 (1993).
[4] G. Ertl, Adv. Catal. **37**, 213 (1990).
[5] M. Ehsasi, M. Berdau, T. Rebitzki, K.-P. Charlé, K. Christmann, and J. H. Block, J. Chem. Phys. **98**, 9177 (1993).
[6] M. Berdau, M. Ehsasi, A. Karpowicz, W. Engel, K. Christmann, and J. H. Block, Vacuum **45**, 271 (1994).
[7] S. Jakubith, H. H. Rotermund, W. Engel, A. von Oertzen, and G. Ertl, Phys. Rev. Lett. **65**, 3013 (1990).
[8] S. Nettesheim, A. von Oertzen, H. H. Rotermund, and G. Ertl, J. Chem. Phys. **98**, 9977 (1993).
[9] R. Imbihl and G. Ertl, Chem. Rev. **95**, 697 (1995).
[10] J. Boissonade and P. de Kepper, J. Phys. Chem. **84**, 501 (1980).
[11] F. Schlögl, Z. Phys. **248**, 446 (1971); **253**, 147 (1972).
[12] F. Schlögl, Ber. Bunsenges. Phys. Chem. **84**, 351 (1980).
[13] P. de Kepper and J. Boissonade, *Oscillations and Traveling Waves in Chemical Systems*, edited by R. J. Field and M. Burger (Wiley, New York, 1985), Chap. 7.
[14] S. D. Furrow, *Oscillations and Traveling Waves in Chemical Systems*, edited by R. J. Field and M. Burger (Wiley, New York, 1985), Chap. 5.
[15] R. J. Field, in *Oscillations and Traveling Waves in Chemical Systems*, edited by R. J. Field and M. Burger (Wiley, New York, 1985), Chap. 2.
[16] Q. Ouyang and P. de Kepper, J. Phys. Chem. **91**, 6040 (1987).
[17] W. Engel, M. E. Kordesch, H. H. Rotermund, S. Kubala, and A. von Oertzen, Ultramicrosc. **36**, 148 (1991).
[18] H. H. Rotermund, W. Engel, M. Kordesch, and G. Ertl, Nature **343**, 355 (1990).
[19] M. Berdau, *Untersuchungen zu Hysterese- und Oszillationserscheinungen bei der katalytischen CO-Oxidation auf Platinmetalloberflächen* (Köster, Berlin, 1994).
[20] M. Berdau, G. G. Yelenin, A. Karpowicz, M. Ehsasi, K. Christmann, and J. H. Block (unpublished).
[21] V. P. Zhdanov and B. Kasemo, Surf. Sci. Rep. **20**, 111 (1994).
[22] M. Bär, Ch. Zülicke, M. Eiswirth, and G. Ertl, J. Chem. Phys. **96**, 8595 (1992).
[23] J. C. Roux, P. de Kepper, and J. Boissonade, Phys. Lett. **97A**, 168 (1983).
[24] R. Bruinsma and G. Aeppli, Phys. Rev. Lett. **52**, 1547 (1984).
[25] G. Parisi, Europhys. Lett. **17**, 673 (1992).
[26] W. Ebeling, A. Engel, L. Schimansky-Geier, and Ch. Zülicke, Physica D **49**, 170 (1991).
[27] A. S. Mikhailov, *Foundations of Synergetics I* (Springer, Berlin, 1990), Chap. 2.
[28] M. Bär, N. Gottschalk, M. Eiswirth, and G. Ertl, J. Chem. Phys. **100**, 1202 (1994).
[29] M. Falcke, M. Bär, H. Engel, and M. Eiswirth, J. Chem. Phys. **97**, 4555 (1992).
[30] M. Sander, R. Imbihl, and G. Ertl, J. Chem. Phys. **95**, 6162 (1991).
[31] G. G. Yelenin, M. Berdau, and K. Christmann (unpublished).
[32] M. Ehsasi, S. Rezaie-Serej, J. H. Block, and K. Christmann, J. Chem. Phys. **92**, 7596 (1990).
[33] M. Berdau *et al.* (unpublished).
[34] M. Sander, G. Veser, and R. Imbihl, J. Vac. Sci. Technol. A **10**, 2495 (1992).
[35] M. Ehsasi, A. Karpowicz, M. Berdau, W. Engel, K. Christmann, and J. H. Block, Ultramicrosc. **49**, 318 (1993).
[36] A. T. Winfree, Sci. Am. **230**, 82 (1974).
[37] G. G. Yelenin and A. G. Makeev, Math. Modeling (in press).
[38] I. R. Epstein, K. Kustin, P. de Kepper, and M. Orbán, Sci. Am. **248**, 96 (March 1983).
[39] S. Moldenhauer *et al.* (unpublished).
[40] K. Krischer, M. Eiswirth, and G. Ertl, Surf. Sci. **251/252**, 900 (1991).
[41] G. G. Yelenin, M. Berdau, K. Christmann, and J. H. Block (in preparation).
[42] N. Hartmann, K. Krischer, and R. Imbihl, J. Chem. Phys. **101**, 6717 (1994).
[43] G. Veser and R. Imbihl, J. Chem. Phys. **100**, 8483 (1994).
[44] J. Lauterbach and H. H. Rotermund, Surf. Sci. **311**, 231 (1994), and (private communication).
[45] M. Ehsasi, M. Berdau, A. Karpowicz, K. Christmann, and J. H. Block, in *Proceedings of the 10th International Congress on Catalysis*, Budapest, 1992, edited by L. Guczi, F. Solymosi, and P. Tétényi (Akadémiai Kiadó, Budapest, 1993), Part B.